

Transcriptional Profiling of Foam Cells Reveals Induction of Guanylate-Binding Proteins Following Western Diet Acceleration of Atherosclerosis in the Absence of Global Changes in Inflammation

Young-Hwa Goo, PhD; Se-Hee Son, PhD; Vijay K. Yechoor, MD; Antoni Paul, PhD

Background—Foam cells are central to two major pathogenic processes in atherogenesis: cholesterol buildup in arteries and inflammation. The main underlying cause of cholesterol deposition in arteries is hypercholesterolemia. This study aimed to assess, in vivo, whether elevated plasma cholesterol also alters the inflammatory balance of foam cells.

Methods and Results—Apolipoprotein E-deficient mice were fed regular mouse chow through the study or were switched to a Western-type diet (WD) 2 or 14 weeks before death. Consecutive sections of the aortic sinus were used for lesion quantification or to isolate RNA from foam cells by laser-capture microdissection (LCM) for microarray and quantitative polymerase chain reaction analyses. WD feeding for 2 or 14 weeks significantly increased plasma cholesterol, but the size of atherosclerotic lesions increased only in the 14-week WD group. Expression of more genes was affected in foam cells of mice under prolonged hypercholesterolemia than in mice fed WD for 2 weeks. However, most transcripts coding for inflammatory mediators remained unchanged in both WD groups. Among the main players in inflammatory or immune responses, chemokine (C-X-C motif) ligand 13 was induced in foam cells of mice under WD for 2 weeks. The interferon-inducible GTPases, guanylate-binding proteins (GBP)3 and GBP6, were induced in the 14-week WD group, and other GBP family members were moderately increased.

Conclusions—Our results indicate that acceleration of atherosclerosis by hypercholesterolemia is not linked to global changes in the inflammatory balance of foam cells. However, induction of GBPs uncovers a novel family of immune modulators with a potential role in atherogenesis. (*J Am Heart Assoc.* 2016;5:e002663 doi: 10.1161/JAHA.115.002663)

Key Words: atherosclerosis • cholesterol • gene expression • inflammation • macrophages

Lipid-laden macrophages, or foam cells, are chief cellular components of atherosclerotic lesions through all stages of development.¹ Circulating monocytes are recruited to the arterial wall in response to inflammatory stimuli induced, among other factors, by modified low-density lipoprotein (mLDL) particles deposited in the subendothelial space. Monocytes differentiate into macrophages that take up mLDL in an unfettered fashion and become heavily loaded with

lipoprotein-derived cholesterol, while they also orchestrate the development of a local inflammatory process.^{2–4} Given that, presumably, the amount of mLDL deposited in arteries is related to the concentration of circulating LDL, it might be inferred that, by promoting monocyte immigration, hypercholesterolemia directly contributes to vascular inflammation.³ However, it could also be possible that exposure to different lipoprotein concentrations alters the inflammatory balance of foam cells. The main LDL modifications related to atherosclerosis development involve lipid peroxidation.⁵ Transcriptional response of macrophages to exposure to oxidized (ox) LDL has been tested in cultured macrophages of different sources, with diverse results that, depending on the study, suggested predominantly proinflammatory or anti-inflammatory effects.^{6–9} In some cases, the outcome was significantly affected by changes in experimental variables, such as the cell type, form of LDL modification and presentation to cells, or time of exposure to the lipoproteins. For example, Brand et al. found that short-term exposure of THP-1 macrophages to oxLDL induced activation of nuclear factor kappa B (NF-κB), whereas long-term exposure to oxLDL not only did not activate NF-κB, but actually prevented NF-κB activation by

From the Center for Cardiovascular Sciences, Albany Medical College, Albany, NY (Y.-H.G., S.-H.S., A.P.); Division of Diabetes, Endocrinology & Metabolism, Department of Medicine, Baylor College of Medicine, Houston, TX (V.K.Y.).

Accompanying Tables S1 and S2 are available at <http://jaha.ahajournals.org/content/5/4/e002663/DC1/embed/inline-supplementary-material-1.pdf>

Correspondence to: Antoni Paul, PhD, Center for Cardiovascular Sciences, Albany Medical College, 47 New Scotland Ave, MC-8, Albany, NY 12208. E-mail: paula@mail.amc.edu

Received September 11, 2015; accepted March 1, 2016.

© 2016 The Authors. Published on behalf of the American Heart Association, Inc., by Wiley Blackwell. This is an open access article under the terms of the Creative Commons Attribution-NonCommercial-NoDerivs License, which permits use and distribution in any medium, provided the original work is properly cited, the use is non-commercial and no modifications or adaptations are made.

lipopolysaccharide¹⁰; Hammad et al. observed different effects on inflammatory gene expression depending on whether U937 monocytic cells were treated with oxLDL or with oxLDL immune complexes¹¹; and Shiffman et al. identified gene clusters in THP-1 macrophages with different temporal patterns of expression in response to treatment with oxLDL. An added challenge that might contribute to the variability of studies on macrophages is the remarkable plasticity of these cells, which allows them to change their phenotype depending on the surrounding environment.¹² Thus, given that the complex atherosclerotic milieu is difficult to reproduce in vitro, cell-culture approaches to characterize macrophages may not represent the functional relevance of the variables being studied as well as studies performed on macrophages resident within actual atherosclerotic lesions.

The apolipoprotein E-deficient (apoE^{-/-}) mouse is a widely used mouse model of atherosclerosis.^{13–15} From a molecular point of view, gene expression patterns in mouse aortas that defined different stages of atherosclerosis development also correlated with severity of human coronary lesions.¹⁶ Like in humans, atherosclerosis development in apoE^{-/-} mice is driven by hypercholesterolemia, and plasma cholesterol levels and the extent of lesion development are directly related to the cholesterol content in their diet.¹⁷ Thus, to study the effect of hypercholesterolemia on the transcriptional response of lesional foam cells, here we have fed apoE^{-/-} mice regular chow through the study or have switched their diet to a Western-type diet (WD) for a short (2 weeks) or for a longer (14 weeks) time period. We have assessed the effects of the WD on atherosclerosis development in cross-sections of the aortic sinus, and we have used sections consecutive to the used for lesion quantification to selectively isolate RNA by laser-capture microdissection (LCM) from lesional macrophages to perform a broad analysis of gene expression, with an emphasis on the expression of genes that regulate inflammatory and immune responses.

Methods

Experimental Design

At 8 weeks of age, 15 female apoE^{-/-} mice in C57BL6/J background were divided into 3 groups with similar cholesterol levels. One group was maintained on regular mouse chow (2020X Teklad Global Soy Protein-Free Extruded Rodent Diet; Harlan Laboratories, Indianapolis, IN) until death at 22 weeks. This is a cholesterol-free diet that provides 3.5 kcal/g, including 16% of calories from fat. From 8 weeks of age to the end of the study, the diet of a second group of 5 mice was switched from regular chow to a WD (TD.88137; Harlan Laboratories). This diet provides 4.5 kcal/g and contains 20% (wt/wt) milk fat (42% of total calories) and

0.15% (wt/wt) cholesterol. The third group of mice remained on regular chow until the age of 20 weeks, when mice were fed WD for the remaining 2 weeks of the study. The study design is summarized in Figure 1A. Cholesterol measurements and lipoprotein fractionation by fast-performance liquid chromatography were performed as we previously described.¹⁸ Plasma oxLDL levels were determined by ELISA (USCN Life Science Inc., Wuhan, China), following the manufacturer's instructions.^{19,20} Additional mice were used to obtain aortic arches for RNA isolation from whole artery, isolate thioglycollate-elicited peritoneal macrophages, and assess the rate of increase of plasma cholesterol upon introduction of the WD. All animal experiments were conducted following protocols approved by the institutional animal care and use committees at Albany Medical College (Albany, NY) and Baylor College of Medicine (Houston, TX).

Lesion Analysis

After death, mouse hearts were perfused with sterile PBS, bisected, and the upper half immediately embedded in OCT (Sakura, Torrance, CA) and stored at -80°C . Approximately 30 consecutive 7- μm cryosections of each aortic sinus were sequentially mounted on 3 slides. The first and third slides, which were used for macrophage isolation by LCM, were immediately fixed, cell nuclei were stained with toluidine blue, and sections were dehydrated with the HistoGene LCM Frozen Section Staining Kit (Applied Biosystems, Foster City, CA). The second slide was stained for macrophages with anti-Lamp2/Mac3 antibody (Santa Cruz Biotechnology, Santa Cruz, CA) and used as a template to identify macrophage-rich areas within the lesions. Images were acquired with a Zeiss AxioObserver.D1 microscope using an AxioCam MRc camera (Carl Zeiss, Jena, Germany), and analyzed with AxioVision software (Zeiss). Lesion area was measured by outlining the perimeter of the area between the vessel lumen and media layer of the arteries. The areas within lesions that stained positive for macrophages were determined using ImageJ software (National Institutes of Health [NIH], Bethesda, MD), as we previously described.²¹

LCM and RNA Amplification

LCM of macrophages and RNA processing were performed as we previously described.²² Briefly, ≈ 2000 laser shots (power, ≈ 65 mV; pulse, ≈ 2500 μs) were performed with a Veritas Microdissection System (Applied Biosystems), and cells were collected on CapSure HS LCM Caps (Applied Biosystems). RNA was extracted with the PicoPure RNA Isolation Kit (Applied Biosystems). mRNA was submitted to 2 rounds of amplification with the RiboAmp HS RNA Amplification Kit (Applied Biosystems), each of which consisted of synthesis of

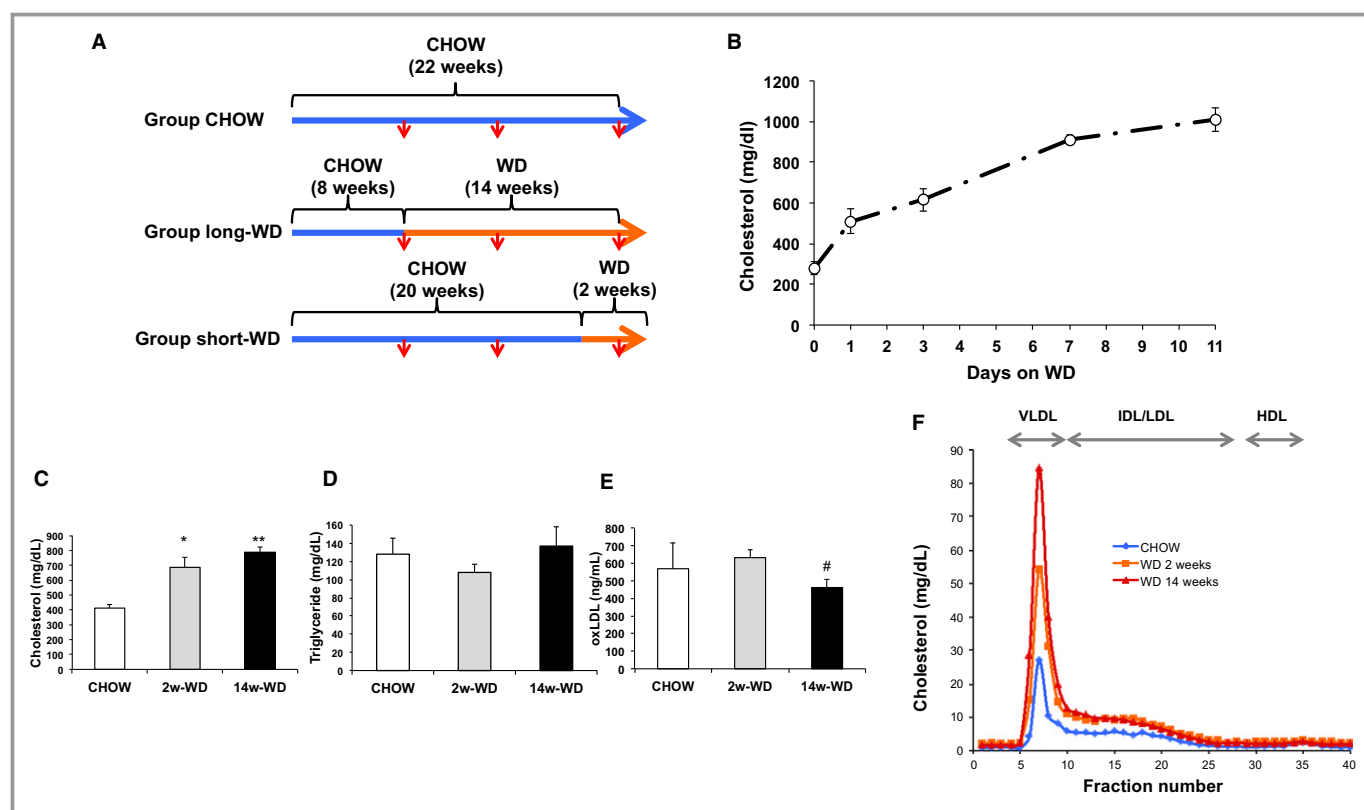


Figure 1. A, Study design. Blue lines represent time periods in which mice were fed regular chow; periods of WD feeding are represented in orange. Red arrows indicate times of blood sampling. B, Time course of plasma cholesterol elevation after introduction of WD. Mice were not fasted for these plasma measurements ($n=5$). C, D, and E, Fasting plasma cholesterol (C), triglyceride (D), and oxLDL (E) levels at time of death in mice used for gene expression studies ($n=5$). F, Cholesterol distribution in different lipoprotein fractions in pooled plasmas obtained at week 22 under overnight fasting. * $P<0.005$ and ** $P<0.001$ with respect to CHOW; # $P<0.05$ with respect to 2-week WD. HDL indicates high-density lipoprotein; IDL, intermediate-density lipoprotein; LDL, low-density lipoprotein; oxLDL, oxidized low-density lipoprotein; VLDL, very low-density lipoprotein; WD, Western-type diet.

double-stranded cDNA using oligo(dT) primers tagged with the T7 promoter sequence, followed by in vitro transcription (IVT) with T7 polymerase.²² A_{260}/A_{280} ratios and size distribution analysis of amplified cRNAs were assessed with an Agilent 2100 bioanalyzer (Agilent Technologies Inc., Santa Clara, CA).

Gene Expression Analysis

Fifteen micrograms of each cRNA were biotin-labeled with the TURBO Labeling Biotin kit (Applied Biosystems), fragmented, and hybridized to Mouse Genome 430 2.0 Arrays (Affymetrix, San Diego, CA), as we previously described.²² Data were filtered with dChip software to include probes with $\geq 50\%$ presence call in the arrays and with expression levels of ≥ 25 in $\geq 50\%$ samples. The filtered data were transferred to MeV software,²³ log₂ transformed, and differential gene expression in the 3 experimental groups was assessed by ANOVA. Welch's t test (assuming unequal variances) was used for pairwise comparisons. Differences were considered significant when $P \leq 0.01$. To visualize the patterns of gene expression

between data sets, volcano plots were generated by plotting significance versus fold change in the Y and X axes, respectively. Pathway Express was used to identify the most relevant pathways affected by the dietary manipulations.²⁴ This software calculates P values based on the number of genes differentially expressed in each pathway in relationship to the number of genes expected to change by chance. It also produces a gamma P value that, in addition to classical statistics, takes into consideration parameters such as the fold change and the topology of genes within each given pathway.²⁴ Thus, the gamma P value is influenced by biologically meaningful factors that are not usually captured by classic statistics.

Primers for quantitative real-time polymerase chain reaction (qPCR) were designed in the 3'-terminus region of mRNA, including the 3' untranslated region (Table). Relative gene expression was determined from threshold cycle values normalized to cyclophilin A, as we previously described.²² For gene expression analyses in cultured primary macrophages, thioglycollate-elicited peritoneal macrophages were

Table. Primer Sequences

Name	Sequence
Cyclophilin A	Forward 5'-TGGTCTTTGGGAAGGTGAAA -3'
	Reverse 5'-CACAGTCGGAAATGGTGATCT-3'
CD68	Forward 5'- CCTCACCTGGTGCTCAT -3'
	Reverse 5'- ATTGATTCCCCACCCCTATT-3'
CD14	Forward 5'- GTGGCCTTGTGAGGAAGTCT -3'
	Reverse 5'- ATCAGGGGTCAAGTTTGCTG -3'
SR-A1	Forward 5'- GCCCTGTTCAGAAGCATCA -3'
	Reverse 5'- CTTGATCAGGACAGCAT -3'
ABCA1	Forward 5'-TGGATCTATTTTGCAGTGA-3'
	Reverse 5'-CAGCAGGACTGTACAGCTTTA-3'
α -actin	Forward 5'- TCAACAGAGGAAGGTCCACTT -3'
	Reverse 5'- ACTTGCCAAATTTAAATACAG -3'
SM22	Forward 5'-CAGAGGAAGCAGGCTATGGA-3'
	Reverse 5'-AACCCAAACAAGTCCACCAC-3'
MYH11	Forward 5'-CACAGGAACTTCGAGTGA-3'
	Reverse 5'-TTCTGTTTTCCCTGACATGGT -3'
VE-cadherin	Forward 5'- AGGAAGGGGCATACAGACAC -3'
	Reverse 5'- CCTGCAGAAAGGCTTGTG -3'
IL-6	Forward 5'-TGACAAATATGAATGTTGGGACA-3'
	Reverse 5'-TTCCAAGAAACCATCTGGCTA-3'
CCL2	Forward 5'-TCCCTCTCTGTGAATCCAGA-3'
	Reverse 5'- ACCTTGAATCTCAAACACAAAG-3'
CXCL13	Forward 5'- CCTGGGGGAAACAGTCTAC -3'
	Reverse 5'- GCCTGGACCTTTAAGCTGAG -3'
TNF- α	Forward 5'-GTCCTGGAGGACCCAGTGT-3'
	Reverse 5'-GGGAGCAGAGGTTCACTGAT-3'
IL-18	Forward 5'- GTTAGTGGGGAGGTTTGT-3'
	Reverse 5'- GCAGCCTCGGGTATTCTGT -3'
GBP3	Forward 5'- ACATGGCCAAATGAAGACACA-3'
	Reverse 5'- TGAAAACCCACTTGTGCGTT-3'
GBP6	Forward 5'- TCATCTTGGTGGTTGGAACA-3'
	Reverse 5'-TCATGAGAAACAATGTCACAAGG-3'
GBP8	Forward 5'- TGAGGGTATTTTCATCACAGCA -3'
	Reverse 5'- TTGCCAATCTAAGTCAAGGATG-3'
GBP4	Forward 5'-CCTTGTGATATTGTTCCACGGT-3'
	Reverse 5'-AATTGGGAAGGTTGCAGGTG-3'
GBP2	Forward 5'- TGTTCTCTTTCTACAGATAGC -3'
	Reverse 5'- AAGTCCTCAGAGAAATGAAAGGG -3'

ABCA1 indicates ATP binding cassette A1; CCL2 indicates chemokine (C-C motif) ligand 2; CXCL, chemokine (C-X-C motif) ligand 13; GBP, guanylate-binding protein; IL, interleukin; MYH11, myosin heavy chain 11; SM22, smooth muscle protein 22; SR-A1, scavenger receptor A1; TNF α , tumor necrosis factor alpha.

cultured in DMEM/0.2% BSA containing oxLDL (1, 50 or 100 μ g/mL; Alfa Aesar, Ward Hill, Ma) for 4 or 24 hours. RNA was purified and digested with DNase using the Absolutely RNA miniprep kit (Agilent Technologies). Reverse transcription of 500 ng of total RNA was performed with SuperScript III (Invitrogen, Carlsbad, CA). The qPCR protocol was the same used for analysis of samples isolated by LCM.

Statistical Analysis

Statistical analysis of nonmicroarray data was carried out using parametric methods when the data followed a normal distribution and the samples had equal variances. Otherwise, nonparametric tests were used for the analysis. When parametric tests were used, multiple comparisons were analyzed by ANOVA, and post-hoc pair-wise comparisons were performed using the Holm–Sidak test. When nonparametric tests were used, multiple comparisons were performed with the Kruskal–Wallis test, followed by pair-wise comparisons with the Mann–Whitney *U* test. Statistical analysis involving comparisons between two groups were performed using a 2-tailed Student *t* test (parametric) or the Mann–Whitney *U* test (nonparametric). Differences were considered significant when $P < 0.05$. Values are presented as mean \pm SEM.

Results

Effects of WD on Plasma Lipids and Atherosclerosis Development

To determine the adequate length of the study in which foam cells were exposed to hypercholesterolemia for a short time period, we performed a preliminary study to assess the rate of increase of plasma cholesterol in apoE^{−/−} mice upon introduction of the WD. As seen in Figure 1B, plasma cholesterol was markedly higher at 24 hours of WD feeding, but levels continued to increase gradually to reach concentrations of ≈ 1000 mg/dL (under fed conditions) at day 11. Thus, in order to expose foam cells to plasma cholesterol levels similar to the achieved under prolonged WD, but for a period of time not long enough to affect atherosclerosis development, mice were fed WD for 2 weeks. Fasting plasma cholesterol levels measured at the time of death in mice used for gene expression studies were still moderately ($\approx 10\%$) higher in mice fed WD for 14 weeks than in mice that were fed WD for only 2 weeks, although these differences did not reach statistical significance. However, in both WD groups, cholesterol levels were significantly (≈ 2 -fold) higher than in mice fed regular mouse chow (Figure 1C and 1F). As expected

in apoE^{-/-} mice, plasma triglycerides did not increase in response to WD (Figure 1D). Although oxidative modifications are believed to take place mainly on apoB-containing lipoproteins retained at the arterial wall, oxLDL is also present in the circulation.^{25,26} Plasma oxLDL were very similar between mice fed chow through the study and mice fed WD for the last 2 weeks, whereas oxLDL levels were slightly reduced in mice fed WD for 14 weeks (Figure 1E). This observation is consistent with recent studies that showed that plasma oxLDL decreases concomitantly with increase in lesion size.²⁶ Indeed, the prolonged hypercholesterolemia in the 14-week WD group resulted in a very substantial (>3-fold) increase in atherosclerosis development at the aortic sinus: $696 \pm 32 \times 10^3 \mu\text{m}^2$ in mice fed WD for 14 weeks versus $221 \pm 13 \times 10^3 \mu\text{m}^2$ in mice fed regular chow through the study. However, the size of the lesions in the 2-week WD group was similar to that of mice fed regular chow: $263 \pm 37 \mu\text{m}^2$ (Figure 2A and 2B). Next, we performed immunohistochemical analyses to quantify the areas of macrophages within lesions. The relative macrophage content was similar in mice fed chow through the study and in mice fed WD for 2 weeks ($\approx 35\text{--}40\%$), but it was lower ($\approx 25\%$) in mice fed WD for 14 weeks (Figure 2C). However, the total area of macrophages, calculated by multiplying the percentage of macrophages by the total lesion area, was higher in mice fed WD for 14 weeks (Figure 2D). Thus, WD feeding for either 2 or 14 weeks significantly increased plasma

cholesterol levels. However, lesions in mice fed WD for 2 week were similar in size and contained a similar amount of macrophages than those of mice fed chow through the study, whereas the longer WD feeding protocol markedly increased the progression of atherosclerotic lesions.

Gene Expression Analyses of Lesional Foam Cells

RNA from lesional foam cells was isolated by LCM and amplified by IVT to obtain enough material for a broad gene expression analysis.²² First, to control the quality of the isolation and amplification processes, we assessed whether the gene expression patterns in the cRNA amplified from cells captured by LCM were the expected in macrophage/foam cell populations. Using qPCR, we compared expression of several macrophage markers between these cRNA samples and cRNA amplified from lysates of aortic arches (whole artery) of apoE^{-/-} mice. As seen in Figure 3A through 3D, levels of transcripts that are typically elevated in macrophage populations, including CD68, CD14, scavenger receptor A1 (SR-A1), and ATP binding cassette A1 (ABCA1), were enriched in LCM-cRNAs. Conversely, levels of transcripts coding for the smooth muscle cell (SMC) markers, α -actin, smooth muscle myosin heavy chain 11 (MYH11), and smooth muscle protein 22 (SM22), were significantly reduced in macrophages isolated by LCM (Figure 3E through 3G). Likewise, mRNA coding for the endothelial cell marker VE-cadherin, was also

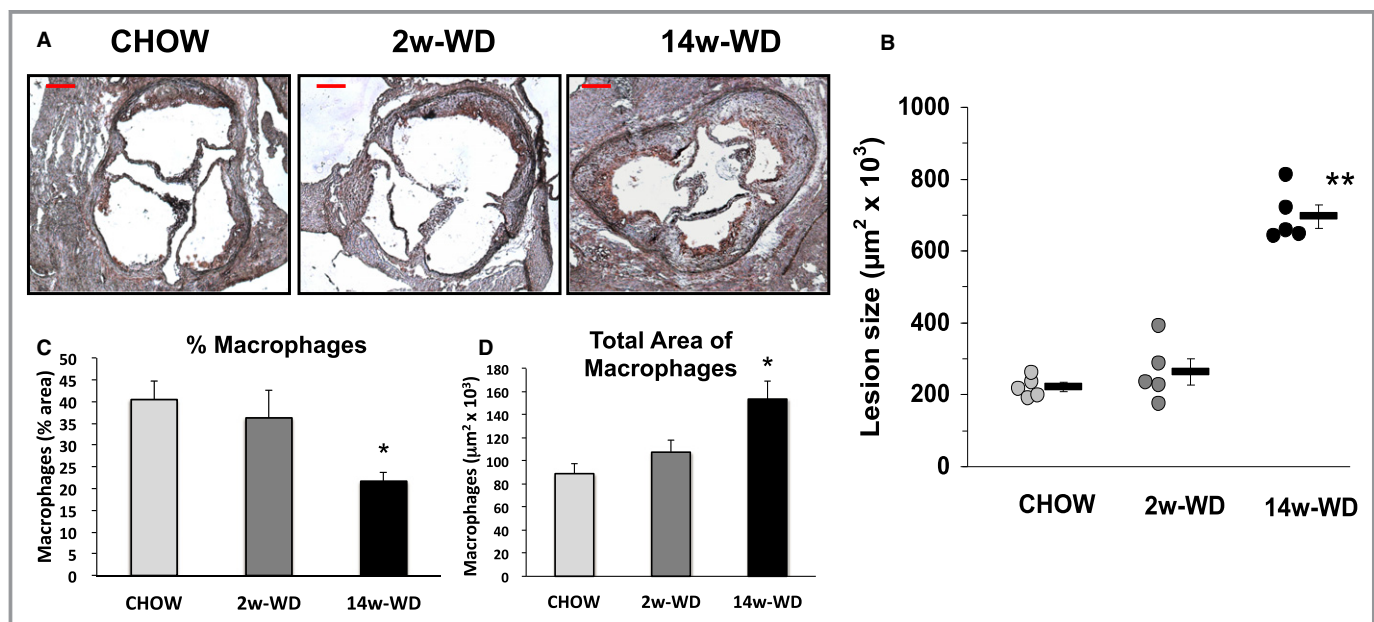


Figure 2. A, Representative images of sections of the aortic sinus in the 3 experimental groups stained with the macrophage marker, Mac-3 (Brown), and counterstained with hematoxylin. Bar=200 μm . B, Area of atherosclerosis involvement was determined by quantifying the area between the media layer and the vessel lumen. Dots represent individual values. Bars represent average \pm SEM. C, Percentage of lesion area occupied by macrophages and (D) absolute of macrophages at the aortic sinus. * $P<0.05$ and ** $P<0.001$ with respect to CHOW. WD indicates Western-type diet.

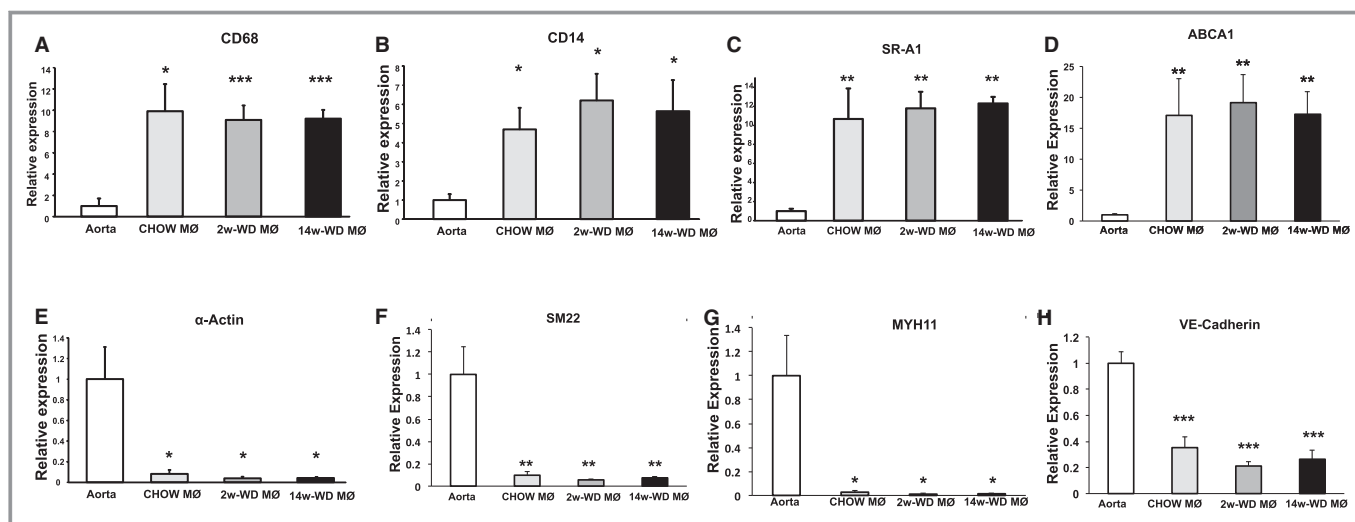


Figure 3. qPCR analysis comparing the expression of genes between RNA isolated from macrophage/foam cell populations (MΦ) by LCM and RNA isolated from aortic arches (aorta). A through D, Are genes highly expressed by foam cells, including CD68 (A), CD14 (B), SR-A1 (C) and ABCA1 (D). E through H, Are markers of other cell types, including the smooth-muscle cell markers α -actin (E), SM22 (F) and MYH11 (G), and the endothelial cell marker VE-cadherin (H). $n=5$. * $P<0.05$, ** $P<0.01$ and *** $P<0.005$ with respect to aorta. LCM indicates laser-capture microdissection; qPCR, quantitative polymerase chain reaction; WD, Western-type diet.

reduced in LCM samples (Figure 3H). Importantly, both the enrichment in macrophage markers and the decrease in SMC markers and VE-cadherin were similar in LCM-cRNAs in the 3 experimental groups.

For broad gene expression profiling of foam cells, amplified cRNAs were biotinylated and hybridized to Affymetrix DNA chips. The microarray data have been deposited at the GEO (Gene Expression Omnibus) repository and can be accessed through the accession number GSE70619. Data was filtered to remove probes with low presence of call and/or low intensity across the board of arrays, and 15 433 targets satisfied the filtering criteria. Among them, ANOVA analysis at a P value of 0.01 followed by pair-wise comparisons against the “CHOW” group identified 52 targets significantly affected in the 2-week WD group and 366 targets in the 14-week WD group. Volcano plots summarizing these changes are shown in Figure 4A and 4B, and the genes affected by the dietary manipulations are listed in Table S1 (2-week WD vs CHOW) and Table S2 (14-week WD vs CHOW). To determine the main biological processes affected in response to hypercholesterolemia, the data were analyzed with Pathway Express. Two pathways, “antigen processing and presentation” and “ubiquitin-mediated proteolysis,” were commonly affected in both WD groups (Figure 4C). Changes in genes in the antigen processing and presentation pathway could be related to the increased uptake of modified lipoproteins by foam cells of mice under WD. The reasons for the over-representation of genes in the ubiquitin-mediated proteolysis pathway are not clear, though it was reported that protein ubiquitination was increased in atherosclerotic plaques, and ubiquitin-mediated

proteolysis was the most over-represented pathway in plaques of diabetic patients.^{27,28} Whereas these two pathways were the only ones affected in the 2-week WD group, the higher number of genes differently expressed in the 14-week WD group was reflected in 11 additional pathways significantly affected in this group (Figure 4C). Given that lesions were more developed in response to prolonged WD, but the plasma lipid profiles were similar in both WD groups, it is likely that changes in the lesional microenvironment contributed to the more-robust changes in gene expression observed in the 14-week WD group. Indeed, the modest changes in gene expression observed in mice fed WD for only 2 weeks suggest that hypercholesterolemia is not a major determinant of transcriptional response of foam cells. However, whether the changes in gene expression were directly related to the plasma cholesterol concentrations, or were the result of other changes in the lesional milieu, neither WD feeding protocol affected the expression of the vast majority of genes in inflammatory and immune response categories. The most noteworthy exceptions were chemokine (C-X-C motif) ligand 13 (CXCL13), which was upregulated in the 2-week WD group by ≈ 4.4 -fold, and two members of the p65 guanylate-binding proteins (GBP) family of interferon-inducible GTPases, GBP3 and GBP6, which were induced in the 14-week WD group by ≈ 3.2 - and ≈ 5.2 -fold, respectively.

Analysis of Inflammatory Mediators

The inflammatory nature of atherosclerosis has been supported by numerous studies, including analysis of gene

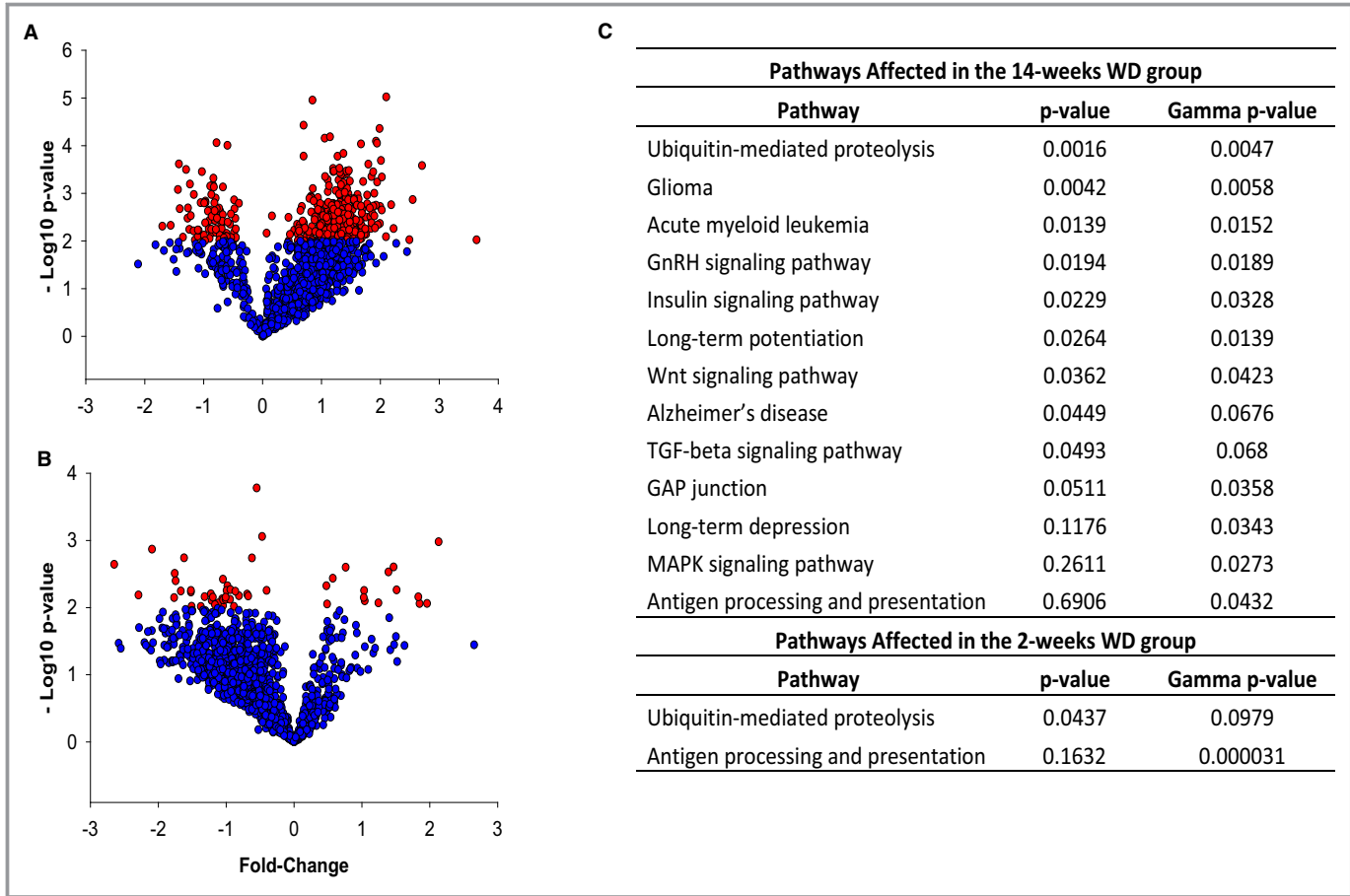


Figure 4. A and B, Volcano plots showing the fold change and level of significance of the genes affected in the 14-week WD group (A) and in the 2-week WD group (B). Red dots represent genes statistically significant at $P<0.01$. C, Pathways affected in foam cells isolated from lesions of mice fed WD for 2 and 14 weeks were determined using Pathway Express. The P value is calculated by a classical analysis based on the set of genes differentially expressed in each pathway related to the number of genes expected to be found by chance. The gamma P value is calculated by an impact analysis that, in addition to classical statistics, includes important biological factors such as fold change and topology of genes within each given pathway. GnRH indicates gonadotropin-releasing hormone; MAPK indicates mitogen-activated protein kinase; TGF, transforming growth factor; WD, Western-type diet.

expression in both clinical samples and animal models of atherosclerosis.^{2,4} Thus, to assess whether genes involved in inflammation could have been affected, but to an extent that did not meet the criteria of this analysis, we performed a similar analysis at a significance level of $P<0.05$ instead of $P<0.01$. As expected, the less-conservative analysis yielded a larger number of genes significantly affected by both dietary manipulations (78 targets significantly changed when comparing 2-week WD vs CHOW and 571 targets when comparing 14-week WD vs CHOW). However, the absence of immune and inflammatory mediators was still evident, and, accordingly, pathways related to the inflammatory and immune responses were not significantly affected (data not shown). Next, we focused the analysis on expression of transcripts coding for major cytokines and chemokines that had been related to progression of atherosclerosis or development of more-severe plaque phenotypes.^{16,28–31} As seen in Figure 5A, in both WD

groups, the levels of most transcripts coding for interleukins or for CC or CXC cytokines were very close or within ≈ 1 -fold change of the levels observed in the CHOW group. There were no obvious trends toward higher or lower ratios in any of the 2 WD groups that suggested an overall proinflammatory or anti-inflammatory effect. Among these players in inflammation, only CXCL13 (in the 2-week WD group) was significantly elevated. This result was confirmed by qPCR analysis (Figure 5B). Interleukin-6 (IL-6) was increased by ≈ 5 -fold in the 14-week WD group, although the signal intensities for IL-6 were very variable and the differences did not reach statistical significance. Changes in IL-6 mRNA levels were not supported by qPCR analysis (Figure 5C). Other inflammatory mediators that displayed modest and nonstatistically significant increases in the microarray analyses, namely, chemokine (C-C motif) ligand 2 (CCL2) in the 2-week WD group or IL-18 in the 14-week WD group, also remained similar among groups

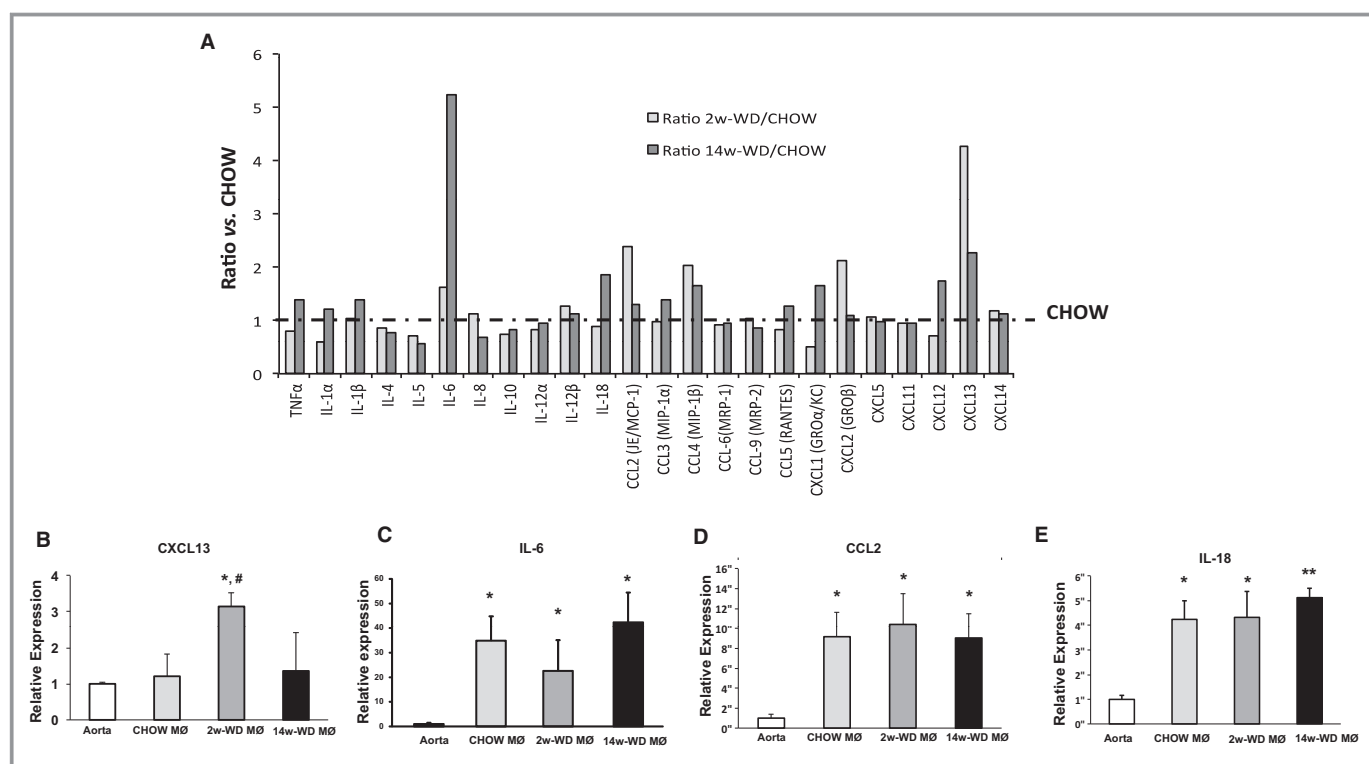


Figure 5. A, Average signal intensity for some of the main macrophage cytokines and chemokines in the microarray analysis. Bars represent the ratios (fold increase) with respect to LCM macrophages in the CHOW group (dashed line). B through E, qPCR analysis of mRNA expression of CXCL13, IL-6, CCL2, and IL-18 in aortas and LCM macrophages of the 3 experimental groups. * $P < 0.05$ and ** $P < 0.001$ with respect to RNA isolated from aortic arches (Aorta); # $P < 0.05$ with respect to CHOW macrophages (MØ). CCL indicates chemokine (C-C motif) ligand; CXCL, chemokine (C-X-C motif) ligand; IL, interleukin; LCM, laser-capture microdissection; qPCR, quantitative polymerase chain reaction; TNF α , tumor necrosis factor alpha; WD, Western-type diet.

by qPCR analysis (Figure 5D and 5E). Interestingly, whereas CXCL13 was induced by short-term hypercholesterolemia, it was not elevated in foam cells from chow-fed mice when compared to whole aortic arches. In contrast, levels of transcripts coding for IL-6, CCL2, and IL-18 were significantly higher in all 3 foam cell populations.

Induction of GBPs by Hypercholesterolemia

A remarkable observation in the microarray analyses was the induction of two p65-GBPs (GBP3 and GBP6) in foam cells of mice fed WD for 14 weeks. Several studies have shown that different GBPs are concomitantly induced.³² Thus, we asked whether in the 14-week WD group there would also be some degree of induction of other GBP family members. Interestingly, as seen in Figure 6A, levels of 5 of the 6 GBPs included in the microarray was higher in foam cells isolated from mice fed WD for 14 weeks than in mice fed regular chow. Intensity of GBP2, GBP7, and GBP8 was ≈ 2 -fold higher, although these differences were not statistically significant. In general, GBPs were not elevated in mice fed WD for only 2 weeks, although GBP6 was relatively higher than in control CHOW-fed mice both in the microarray and qPCR analyses (Figure 6A and 6C).

Results of qPCR analyses were consistent with the microarray data (Figure 6B through 6F). Next, we asked whether the changes observed in vivo would also be observed in vitro in peritoneal macrophages treated with oxLDL. It was reported that oxLDL in human endarterectomy specimens was nearly 70 times higher than plasma oxLDL in the same patients.³³ Thus, given that measurements of oxLDL concentrations within mouse atherosclerotic lesions are extremely challenging, we performed a dose-response study that included a low dose of oxLDL close to the circulating levels (1 $\mu\text{g/mL}$) and 2 higher doses of 50 and 100 $\mu\text{g/mL}$. Mouse peritoneal macrophages were exposed to these concentrations of oxLDL for 4 and 24 hours. None of the treatments altered the levels of the CXCL13 mRNA. However, as seen in Figure 7A, we observed significantly increased GBP3 and GBP6 mRNA in peritoneal macrophages cultured with 100 $\mu\text{g/mL}$ of oxLDL. Overall, GBP6 seems to be the most responsive GBP family member both in vivo and in vitro. Next, we assessed whether expression of other GBP family members was also induced in response to oxLDL, and found that GBP2 and GBP7 were also increased upon treatment with oxLDL (100 $\mu\text{g/mL}$). Thus, whereas CXCL13 was not induced by oxLDL in vitro, several GBP family members were induced, suggesting that oxLDL

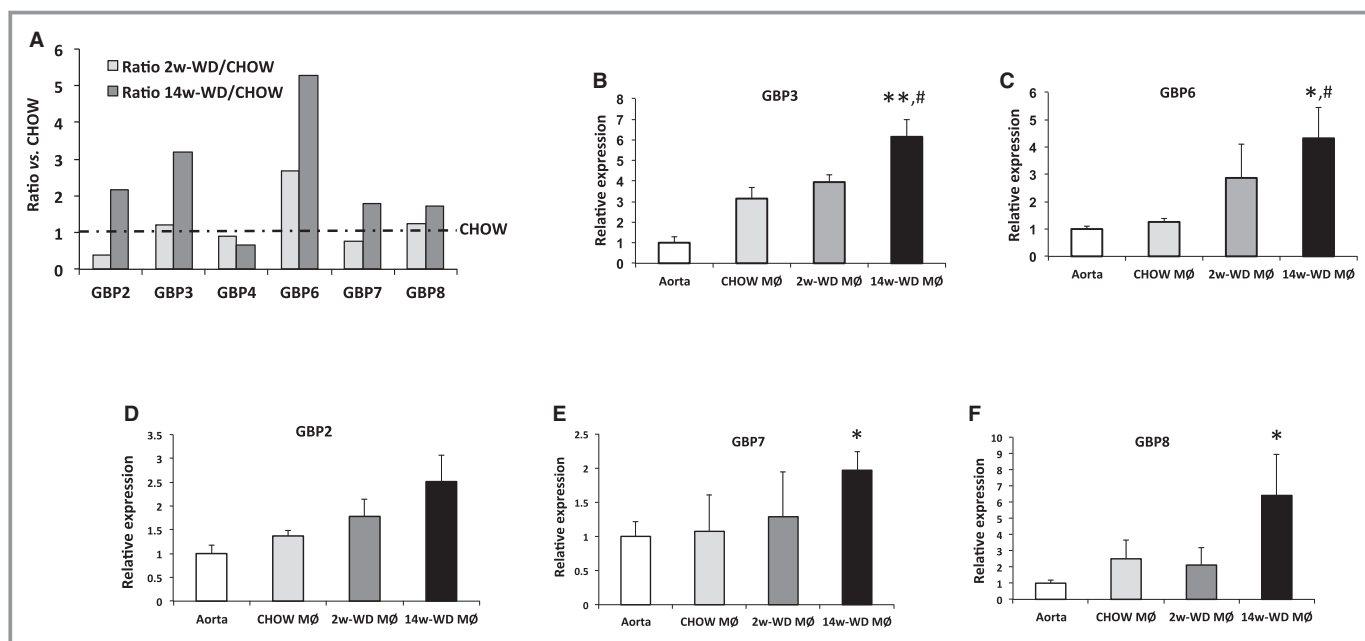


Figure 6. A, Average signal intensity for GBPs present in the microarray. Bars represent the ratios (fold increase) with respect to LCM macrophages in the CHOW group (dashed line). B through F, qPCR analysis of expression of GBP3, GBP6, GBP2, GBP7, and GBP8 in aortas and LCM macrophages of the 3 experimental groups. * $P < 0.05$ and ** $P < 0.001$ with respect to RNA isolated from aortic arches (Aorta); # $P < 0.05$ with respect to CHOW macrophages (MØ). GBP indicates guanylate-binding protein; LCM, laser-capture microdissection; qPCR, quantitative polymerase chain reaction; WD, Western-type diet.

might be one of the factors involved in the induction of GBPs in response to hypercholesterolemia.

Discussion

Hypercholesterolemia is a leading risk factor for development of atherosclerosis, an inflammatory disease of the arterial

wall.² There is compelling evidence supporting the notion that hypercholesterolemia enhances vascular inflammation, including gene expression profiles of aortic sinuses isolated from apoE^{-/-} mice that showed increased expression of inflammatory mediators after the introduction of a Western diet.^{30,34} Upregulation of proinflammatory genes observed in these studies could be the logical consequence of the increased

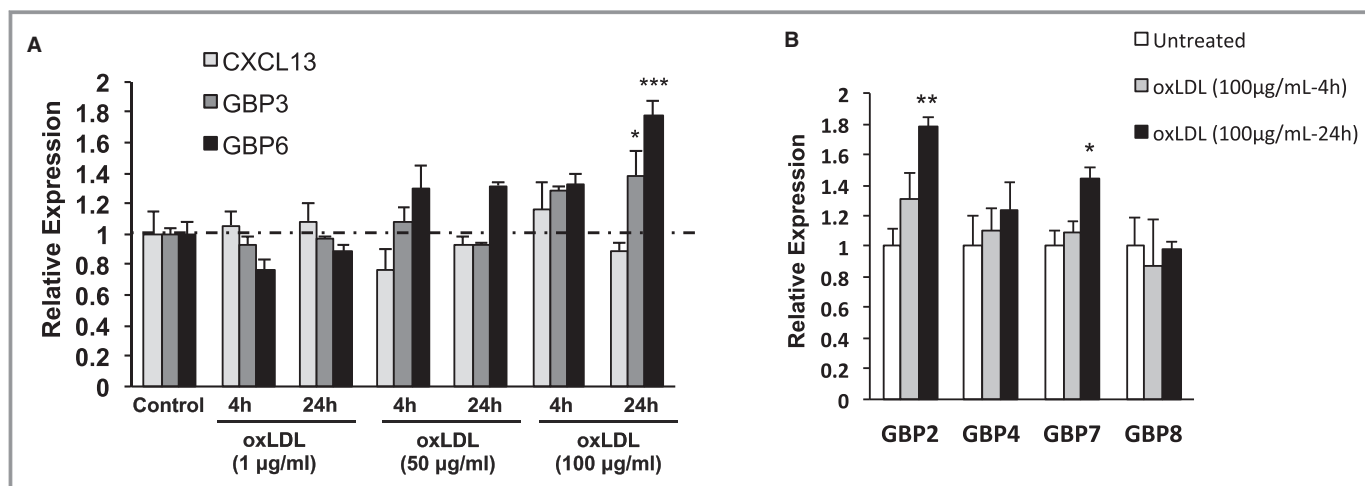


Figure 7. A, qPCR analysis of expression of CXCL13, GBP3, and GBP6 in mouse peritoneal macrophages that remained untreated or were stimulated with oxLDL (1, 50, or 100 µg/mL) for 4 or 24 hours. B, Expression of other GBP family members in response to oxLDL (100 µg/mL for 4 or 24 hours; n=3). * $P < 0.05$, ** $P < 0.01$ and *** $P < 0.001$ with respect to untreated control. CXCL, chemokine (C-X-C motif) ligand; GBP, guanylate-binding protein; oxLDL, oxidized low-density lipoprotein; qPCR, quantitative polymerase chain reaction.

influx of inflammatory cells to the arterial wall during progression of the disease, but could also be related to other factors, such as the activation of lesional cells, in response to hypercholesterolemia. In this line, there is evidence that exposure to modified lipoproteins might regulate the inflammatory response of foam cells. For example, oxLDL was shown to activate NF- κ B by binding to Toll-like receptors (TLRs) such as TLR2 and TLR4.^{35,36} Accumulation of cholesterol crystals in the cytoplasm of macrophages was also proposed to stimulate a proinflammatory cascade.³⁷ Alternatively, lipoprotein-derived oxysterols are natural liver X receptor ligands, which can counter-regulate induction of inflammatory gene expression by NF- κ B by recruiting corepressors to the promoters of inflammatory genes.^{37–39} Thus, we asked whether increases in plasma cholesterol that significantly accelerate atherosclerosis development would actually affect the inflammatory balance of lesional foam cells. Answering this question using complex heterogeneous samples, such as fragments of atheromatous plaques or diseased arteries, may be quite challenging, mainly because of the variable number of inflammatory cells that can be found in these specimens. To circumvent this challenge, here we have used LCM to specifically isolate and assess the inflammatory status of macrophages resident within atherosclerotic lesions. We fed apoE^{−/−} mice for a period of time that was not long enough to affect the size of atherosclerotic lesions (2 weeks) or for a longer period that significantly enhanced the development of atherosclerosis (14 weeks). Whereas WD feeding resulted in a \approx 2-fold elevation in plasma cholesterol, neither dietary manipulation affected expression of the vast majority of genes coding for inflammatory mediators. Thus, a first and foremost conclusion of this study is that accelerated development of atherosclerosis in response to hypercholesterolemia was not linked to major changes in the inflammatory balance of foam cells, as it would be expected if the activity of central regulators of inflammation, such as NF- κ B, were affected.

Although we did not observe global changes in inflammation, we observed certain changes that might be relevant to the pathogenesis of the disease. Expression of the chemokine CXCL13, was elevated only in the short-term WD group. CXCL13 is a homeostatic chemokine that has been primarily linked to lymphocyte trafficking, but has also been shown to influence other key processes such as activation of T cells and macrophages.⁴⁰ CXCL13 is produced by macrophages and is expressed in human atherosclerotic lesions.^{40,41} However, its role in atherogenesis remains poorly characterized, and it has actually been proposed to play a role both in plaque stabilization and plaque destabilization.^{40–42} It is noteworthy that the *in vivo* changes in CXCL13 expression were not recapitulated in peritoneal macrophages cultured with various doses of oxLDL. This may simply stress the importance of

performing gene expression analyses on macrophages within actual atheroma, but could also indicate that CXCL13 expression is induced by other factors involved in the pathogenesis of atherosclerosis.

In the long-term WD group, we observed a significant induction of 2 GBPs, GBP3 and GBP6, as well as a more-moderate elevation of other GBP family members. The GBPs were among the first interferon (IFN)-inducible genes identified, and, like other interferon target genes, the function of GBPs has been primarily associated to protection against viral and bacterial infections.^{43,44} Although their mechanism of action is still under investigation, p65-GBPs have been shown to localize to vacuoles containing pathogens and play a role in transport of autophagic machinery, antimicrobial peptides, and NADPH oxidase (NOX) enzymes for assembly on phagosomal membranes.^{44,45} Interestingly, both the phagocytic clearance of apoptotic cells, known as efferocytosis, and the production of reactive oxygen species by NOX enzymes are processes associated with the development of atherosclerosis.^{46,47} Furthermore, similar to what happens during bacterial phagocytosis, efferocytosis was shown to induce an oxidative burst in macrophages in a NOX-dependent fashion.^{48,49} Importantly, in follow-up studies using cultured macrophages, we found that several GBPs were induced *in vitro* by oxLDL, which indicates that oxLDL may be one of the factors responsible for the induction observed *in vivo*. However, the reason for the specific upregulation of GBPs among the various players in inflammation and immunity is not clear. A possible explanation is that the genes coding for GBPs may be more sensitive to modest changes in inflammation that may take place in more-advanced lesions. Indeed, GBPs are known to be very strongly induced by IFN and other inflammatory stimuli, a fact that even facilitated the characterization of signaling pathways such as the Janus kinase/signal transducer and activator of transcription and the IFN- γ and IFN- α / β pathways.³² However, to our knowledge, this is the first report linking this family of IFN-induced GTPases with the pathogenesis of atherosclerosis. Thus, additional studies will be necessary to determine whether GBPs play a significant role in regulation of atherogenesis, whether it is through regulation of macrophage function during efferocytosis or by other mechanisms.

In conclusion, this study challenges the notion that acceleration of atherogenesis by hypercholesterolemia is linked to a global impact on the inflammatory balance of foam cells. Significant changes among inflammatory and immune mediators included induction of CXCL13 in response to short-term increases in plasma cholesterol, and induction of GBPs in foam cells resident within the more-advanced lesions that formed in response to prolonged hypercholesterolemia. Further research will be necessary to elucidate the role of these players in the development of atherosclerosis.

Acknowledgments

We thank the members of the Genomic and RNA Profiling Core at Baylor College of Medicine for their help in sample processing and discussion.

Sources of Funding

This work was supported by NIH grants HL104251 (to Paul) and R01DK097160 (to Yechoor). Goo was partly supported by an American Heart Association Scientist Development Grant (14SDG19690016).

Disclosures

None.

References

- Glass CK, Witztum JL. Atherosclerosis: the road ahead. *Cell*. 2001;104:503–516.
- Ross R. Atherosclerosis—an inflammatory disease. *N Engl J Med*. 1999;340:115–126.
- Steinberg D. Atherogenesis in perspective: hypercholesterolemia and inflammation as partners in crime. *Nat Med*. 2002;8:1211–1217.
- Libby P. Inflammation in atherosclerosis. *Arterioscler Thromb Vasc Biol*. 2012;32:2045–2051.
- Steinberg D. The LDL modification hypothesis of atherogenesis: an update. *J Lipid Res*. 2009;50:S376–S381.
- Tuomisto TT, Riekkinen MS, Viita H, Levenon AL, Yla-Herttuala S. Analysis of gene and protein expression during monocyte-macrophage differentiation and cholesterol loading—cDNA and protein array study. *Atherosclerosis*. 2005;180:283–291.
- Eligini S, Colli S, Basso F, Sironi L, Tremoli E. Oxidized low density lipoprotein suppresses expression of inducible cyclooxygenase in human macrophages. *Arterioscler Thromb Vasc Biol*. 1999;19:1719–1725.
- Conway JP, Kinter M. Proteomic and transcriptomic analyses of macrophages with an increased resistance to oxidized low density lipoprotein (oxLDL)-induced cytotoxicity generated by chronic exposure to oxLDL. *Mol Cell Proteomics*. 2005;4:1522–1540.
- Spann NJ, Garmire LX, McDonald JG, Myers DS, Milne SB, Shibata N, Reichart D, Fox JN, Shaked I, Heudobler D, Raetz CR, Wang EW, Kelly SL, Sullards MC, Murphy RC, Merrill AH Jr, Brown HA, Dennis EA, Li AC, Ley K, Tsimikas S, Fahy E, Subramaniam S, Quehenberger O, Russell DW, Glass CK. Regulated accumulation of desmosterol integrates macrophage lipid metabolism and inflammatory responses. *Cell*. 2012;151:138–152.
- Brand K, Eisele T, Kreusel U, Page M, Page S, Haas M, Gerling A, Kaltschmidt C, Neumann F-J, Mackman N, Baeuerle PA, Walli AK, Neumeier D. Dysregulation of monocytic nuclear factor- κ B by oxidized low-density lipoprotein. *Arterioscler Thromb Vasc Biol*. 1997;17:1901–1909.
- Hammad SM, Twal WO, Barth JL, Smith KJ, Saad AF, Virella G, Argraves WS, Lopes-Virella MF. Oxidized LDL immune complexes and oxidized LDL differentially affect the expression of genes involved with inflammation and survival in human U937 monocytic cells. *Atherosclerosis*. 2009;202:394–404.
- Verschoor C, Puchta A, Bowdish DM. The Macrophage. *Methods Mol Biol*. 2012;844:139–156.
- Reddick RL, Zhang SH, Maeda N. Atherosclerosis in mice lacking apo E. Evaluation of lesional development and progression. *Arterioscler Thromb*. 1994;14:141–147.
- Zhang SH, Reddick RL, Piedrahita JA, Maeda N. Spontaneous hypercholesterolemia and arterial lesions in mice lacking apolipoprotein E. *Science*. 1992;258:468–471.
- Meir KS, Leitersdorf E. Atherosclerosis in the apolipoprotein E-deficient mouse: a decade of progress. *Arterioscler Thromb Vasc Biol*. 2004;24:1006–1014.
- Tabibiazar R, Wagner RA, Ashley EA, King JY, Ferrara R, Spin JM, Sanan DA, Narasimhan B, Tibshirani R, Tsao PS, Efron B, Quertermous T. Signature patterns of gene expression in mouse atherosclerosis and their correlation to human coronary disease. *Physiol Genomics*. 2005;22:213–226.
- Getz GS, Reardon CA. Diet and murine atherosclerosis. *Arterioscler Thromb Vasc Biol*. 2006;26:242–249.
- Paul A, Chang BH, Li L, Yechoor VK, Chan L. Deficiency of adipose differentiation-related protein impairs foam cell formation and protects against atherosclerosis. *Circ Res*. 2008;102:1492–1501.
- Douglas G, Bendall JK, Crabtree MJ, Tatham AL, Carter EE, Hale AB, Channon KM. Endothelial-specific Nox2 overexpression increases vascular superoxide and macrophage recruitment in ApoE(–/–) mice. *Cardiovasc Res*. 2012;94:20–29.
- Harmon EY, Fronhofer V, Keller RS, Feustel PJ, Zhu X, Xu H, Avram D, Jones DM, Nagarajan S, Lennartz MR. Anti-inflammatory immune skewing is atheroprotective: ApoE(–/–)FcyR1b(–/–) mice develop fibrous carotid plaques. *J Am Heart Assoc*. 2014;3:e001232 doi: 10.1161/JAHA.114.001232.
- Son S-H, Goo Y-H, Choi M, Saha PK, Oka K, Chan LCB, Paul A. Enhanced atheroprotection and lesion remodelling by targeting the foam cell and increasing plasma cholesterol acceptors. *Cardiovasc Res*. 2016;109:294–304.
- Paul A, Yechoor V, Raja R, Li L, Chan L. Microarray gene profiling of laser-captured cells: a new tool to study atherosclerosis in mice. *Atherosclerosis*. 2008;200:257–263.
- Saeed AI, Sharov V, White J, Li J, Liang W, Bhagabati N, Braisted J, Klapa M, Currier T, Thiagarajan M, Sturm A, Snuffin M, Rezantsev A, Popov D, Ryltsov A, Kostukovich E, Borisovsky I, Liu Z, Vinsavich A, Trush V, Quackenbush J. TM4: a free, open-source system for microarray data management and analysis. *Biotechniques*. 2003;34:374–378.
- Draghici S, Khatri P, Tarca AL, Amin K, Done A, Voichita C, Georgescu C, Romero R. A systems biology approach for pathway level analysis. *Genome Res*. 2007;17:1537–1545.
- Tabas I, Williams KJ, Borén J. Subendothelial lipoprotein retention as the initiating process in atherosclerosis: update and therapeutic implications. *Circulation*. 2007;116:1832–1844.
- Itabe H, Obama T, Kato R. The dynamics of oxidized LDL during atherogenesis. *J Lipids*. 2011;2011:418313.
- Wang Z, Guo D, Yang B, Wang J, Wang R, Wang X, Zhang Q. Integrated analysis of microarray data of atherosclerotic plaques: modulation of the ubiquitin-proteasome system. *PLoS One*. 2014;9:e110288.
- King JY, Ferrara R, Tabibiazar R, Spin JM, Chen MM, Kuchinsky A, Vailaya A, Kincaid R, Tsalenko A, Deng DX, Connolly A, Zhang P, Yang E, Watt C, Yakhini Z, Ben-Dor A, Adler A, Bruhn L, Tsao P, Quertermous T, Ashley EA. Pathway analysis of coronary atherosclerosis. *Physiol Genomics*. 2005;23:103–118.
- Satterthwaite G, Francis SE, Suvarna K, Blakemore S, Ward C, Wallace D, Braddock M, Crossman D. Differential gene expression in coronary arteries from patients presenting with ischemic heart disease: further evidence for the inflammatory basis of atherosclerosis. *Am Heart J*. 2005;150:488–499.
- Lutgens E, Faber B, Schapira K, Evelo CT, van Haften R, Heeneman S, Cleutjens KB, Bijnens AP, Beckers L, Porter JG, Mackay CR, Rennert P, Bailey V, Jarpe M, Dolinski B, Kotliansky V, de Fougerolles T, Daemen MJ. Gene profiling in atherosclerosis reveals a key role for small inducible cytokines: validation using a novel monocyte chemoattractant protein monoclonal antibody. *Circulation*. 2005;111:3443–3452.
- Cagnin S, Biscuola M, Patuzzo C, Trabetti E, Pasquali A, Laveder P, Faggian G, Iafrancesco M, Mazzucco A, Pignatti PF, Lanfranchi G. Reconstruction and functional analysis of altered molecular pathways in human atherosclerotic arteries. *BMC Genom*. 2009;10:13.
- Martens S, Howard J. The interferon-inducible GTPases. *Annu Rev Cell Dev Biol*. 2006;22:559–589.
- Nishi K, Itabe H, Uno M, Kitazato KT, Horiguchi H, Shinno K, Nagahiro S. Oxidized LDL in carotid plaques and plasma associates with plaque instability. *Arterioscler Thromb Vasc Biol*. 2002;22:1649–1654.
- Castro C, Campistol JM, Barettino D, Andres V. Transcriptional profiling of early onset diet-induced atherosclerosis in apolipoprotein E-deficient mice. *Front Biosci*. 2005;10:1932–1945.
- Miller YI, Viriyakosol S, Binder CJ, Feramisco JR, Kirkland TN, Witztum JL. Minimally modified LDL binds to CD14, induces macrophage spreading via TLR4/MD-2, and inhibits phagocytosis of apoptotic cells. *J Biol Chem*. 2003;278:1561–1568.
- Hansson GK, Hermansson A. The immune system in atherosclerosis. *Nat Immunol*. 2011;12:204–212.
- Im SS, Osborne TF. Liver X receptors in atherosclerosis and inflammation. *Circ Res*. 2011;108:996–1001.

38. Joseph SB, Castrillo A, Laffitte BA, Mangelsdorf DJ, Tontonoz P. Reciprocal regulation of inflammation and lipid metabolism by liver X receptors. *Nat Med*. 2003;9:213–219.
39. Shibata N, Glass CK. Regulation of macrophage function in inflammation and atherosclerosis. *J Lipid Res*. 2009;50:S277–S281.
40. Smedbakken LM, Halvorsen B, Daissormont I, Ranheim T, Michelsen AE, Skjelland M, Sagen EL, Folkersen L, Krohg-Sorensen K, Russell D, Holm S, Ueland T, Fevang B, Hedin U, Yndestad A, Gullestad L, Hansson GK, Biessen EA, Aukrust P. Increased levels of the homeostatic chemokine CXCL13 in human atherosclerosis—potential role in plaque stabilization. *Atherosclerosis*. 2012;224:266–273.
41. Carlsen HS, Baekkevold ES, Morton HC, Haraldsen G, Brandtzaeg P. Monocyte-like and mature macrophages produce CXCL13 (B cell-attracting chemokine 1) in inflammatory lesions with lymphoid neogenesis. *Blood*. 2004;104:3021–3027.
42. van Dijk RA, Duiniveld AJ, Schaapherder AF, Mulder-Stapel A, Hamming JF, Kuiper J, de Boer OJ, van der Wal AC, Kolodgie FD, Virmani R, Lindeman JH. A change in inflammatory footprint precedes plaque instability: a systematic evaluation of cellular aspects of the adaptive immune response in human atherosclerosis. *J Am Heart Assoc*. 2015;4:e001403 doi: 10.1161/JAHA.114.001403.
43. Carter CC, Gorbacheva VY, Vestal DJ. Inhibition of VSV and EMCV replication by the interferon-induced GTPase, mGBP-2: differential requirement for wild-type GTP binding domain. *Arch Virol*. 2005;150:1213–1220.
44. Kim B-H, Shenoy AR, Kumar P, Das R, Tiwari S, MacMicking JD. A family of IFN- γ -inducible 65-kD GTPases protects against bacterial infection. *Science*. 2011;332:717–721.
45. Dupont CD, Hunter CA. Guanylate-binding proteins: niche recruiters for antimicrobial effectors. *Immunity*. 2012;37:191–193.
46. Thorp E, Subramanian M, Tabas I. The role of macrophages and dendritic cells in the clearance of apoptotic cells in advanced atherosclerosis. *Eur J Immunol*. 2011;41:2515–2518.
47. Lassègue B, San Martín A, Griendling KK. Biochemistry, physiology, and pathophysiology of NADPH oxidases in the cardiovascular system. *Circ Res*. 2012;110:1364–1390.
48. Lee H-N, Surh Y-J. Resolvin D1-mediated NOX2 inactivation rescues macrophages undertaking efferocytosis from oxidative stress-induced apoptosis. *Biochem Pharmacol*. 2013;86:759–769.
49. Yvan-Charvet L, Pagler TA, Seimon TA, Thorp E, Welch CL, Witztum JL, Tabas I, Tall AR. ABCA1 and ABCG1 protect against oxidative stress-induced macrophage apoptosis during efferocytosis. *Circ Res*. 2010;106:1861–1869.

SUPPLEMENTAL MATERIAL

Table S1. Genes differentially expressed in foam cells of mice fed WD for 2 weeks with respect to mice fed regular chow through the entire study.

Affymetrix Probe ID	Fold Change	Gene Symbol	Gene Name
1448859_at	4.38	Cxcl13	chemokine (C-X-C motif) ligand 13
1439276_at	3.89	Adar	adenosine deaminase, RNA-specific
1424436_at	3.60	Gart	phosphoribosylglycinamide formyltransferase
1431028_a_at	3.56	Pank1	pantothenate kinase 1
1431544_at	2.85	4930524B17Rik	
1451381_at	2.76	1810020D17Rik	RIKEN cDNA 1810020D17 gene
1421290_at	2.62	Hspb7	heat shock protein family, member 7
1444328_at	2.37	Clta	chlathrin, light polypeptide
1424713_at	2.06	Calml4	calmodulin-like 4
1424428_at	2.05	Ino80e	INO80 complex subunit E
1453320_at	2.04	1700027A23Rik	RIKEN cDNA 1700027A23 gene
1448104_at	1.69	Aldh6a1	aldehyde dehydrogenase family 6, subfamily A1
1420691_at	1.49	Il2ra	interleukin 2 receptor, alpha chain
1442004_at	1.40	Trim65	tripartite motif-containing 65
1435091_at	1.39	Zfp568	zinc finger protein 568
1434251_at	-1.32	Cnot1	CCR4-NOT transcription complex, subunit 1
1426446_at	-1.39	6430548M08Rik	RIKEN cDNA 6430548M08 gene
1431420_s_at	-1.47	Prelid1	PRELI domain containing 1
1428760_at	-1.54	Snopc3	small nuclear RNA activating complex, polypeptide 3
1433621_at	-1.60	Wdr41	WD repeat domain 41
1417226_at	-1.62	Fbxw4	F-box and WD-40 domain protein 4
1421888_x_at	-1.76	Aplp2	amyloid beta (A4) precursor-like protein 2
1440168_x_at	-1.82	Kctd7	potassium channel tetramerisation domain containing 7
1415911_at	-1.85	Impact	imprinted and ancient
1431716_at	-1.92	Herc4	hect domain and RLD 4
1435867_at	-1.92	Jhdm1d	jumonji C domain-containing histone demethylase 1 homolog D
1418971_x_at	-1.98	Bcl10	B-cell leukemia/lymphoma 10
1423899_at	-1.99	Trip12	thyroid hormone receptor interactor 12
1434660_at	-2.01	Alkbh1	alkB, alkylation repair homolog 1
1437361_at	-2.01	OTTMUSG00000002043	predicted gene, OTTMUSG00000002043
1450905_at	-2.06	Plxnc1	plexin C1
1423066_at	-2.07	Dnmt3a	DNA methyltransferase 3A
1452769_at	-2.07	Rnf145	ring finger protein 145
1417622_at	-2.08	Slc12a2	solute carrier family 12, member 2
1426227_s_at	-2.17	Vps37c	vacuolar protein sorting 37C
1449347_a_at	-2.24	Xlr4c	X-linked lymphocyte-regulated 4B

1437087_at	-2.29	2210408K08Rik	
1424129_at	-2.32	Mfsd1	major facilitator superfamily domain containing 1
1436157_at	-2.34	Ccar1	cell division cycle and apoptosis regulator 1
1448568_a_at	-2.49	Slc20a1	solute carrier family 20, member 1
1423569_at	-2.59	Gatm	glycine amidinotransferase
1416324_s_at	-2.85	Kctd20	potassium channel tetramerisation domain containing 20
1460243_at	-2.87	Sptlc2	serine palmitoyltransferase, long chain base subunit 2
1439251_at	-2.87	100042616	predicted gene, 100042616
1435390_at	-3.08	Exod1	exonuclease domain containing 1
1426894_s_at	-3.18	Fam102a	family with sequence similarity 102, member A
1451798_at	-3.35	Il1rn	interleukin 1 receptor antagonist
1449363_at	-3.38	Atf3	activating transcription factor 3
1448883_at	-3.40	Lgmn	legumain
1440342_at	-4.27	G530011O06Rik	
1422650_a_at	-4.90	Riok3	RIO kinase 3 (yeast)
1435539_at	-6.28	N/A	N/A

Table S2. Genes differentially expressed in foam cells of mice fed WD for 14 weeks with respect to mice fed regular chow through the entire study.

Affymetrix Probe ID	Fold Change	Gene Symbol	Gene Name
1457566_at	12.40	Zfp677	zinc finger protein 677
1428600_at	6.53	Nin	ninein
1435422_at	5.85	4933433P14Rik	RIKEN cDNA 4933433P14 gene
1439363_at	5.63	1200014J11Rik	RIKEN cDNA 1200014J11 gene
1438676_at	5.28	Mpa2l	macrophage activation 2 like
1452833_at	4.67	Rapgef2	Rap guanine nucleotide exchange factor (GEF) 2
1422492_at	4.54	Cpox	coproporphyrinogen oxidase
1438643_at	4.28	Camk1d	calcium/calmodulin-dependent protein kinase ID
1439276_at	4.27	Adar	adenosine deaminase, RNA-specific
1445702_x_at	4.07	Ppapdc2	phosphatidic acid phosphatase type 2 domain containing 2
1452960_at	4.07	Scyl3	SCY1-like 3
1452232_at	4.03	Galnt7	UDP-N-acetyl-alpha-D-galactosamine: polypeptide N-acetylgalactosaminyltransferase 7
1416866_at	3.99	Bet1	blocked early in transport 1 homolog
1425327_at	3.98	Fam76a	family with sequence similarity 76, member A
1427990_at	3.96	Usp45	ubiquitin specific petidase 45
1460389_at	3.88	Cdk8	cyclin-dependent kinase 8
1427938_at	3.85	Mycbp	c-myc binding protein
1436736_x_at	3.84	D0H4S114	DNA segment, human D4S114
1423408_a_at	3.80	2500003M10Rik	RIKEN cDNA 2500003M10 gene
1435164_s_at	3.80	Uba3	ubiquitin-like modifier activating enzyme 3
1456060_at	3.75	Maf	avian musculoaponeurotic fibrosarcoma (v-maf) AS42 oncogene homolog
1460391_at	3.73	Ola1	Obg-like ATPase 1
1452593_a_at	3.72	Tceb1	transcription elongation factor B (SIII), polypeptide 1
1429519_at	3.68	Fpgt	fucose-1-phosphate guanylyltransferase
1424436_at	3.68	Gart	phosphoribosylglycinamide formyltransferase
1433730_at	3.68	Elmod2	ELMO domain containing 2
1437901_a_at	3.65	Vps41	vacuolar protein sorting 41
1451572_a_at	3.60	Mff	mitochondrial fission factor
1456319_at	3.60	N/A	N/A
1436048_at	3.58	Exoc8	exocyst complex component 8
1424360_at	3.56	BC019943	
1435694_at	3.53	Arhgap26	Rho GTPase activating protein 26
1428453_at	3.47	Nat12	N-acetyltransferase 12
1426669_at	3.43	Cpped1	Vcalcineurin-like phosphoesterase domain containing 1
1452047_at	3.43	Cacybp	calcyclin binding protein
1434853_x_at	3.38	Mkrn1	makorin, ring finger protein, 1
1424099_at	3.38	Gpx8	glutathione peroxidase 8

1453071_s_at	3.35	Kdelc2	KDEL (Lys-Asp-Glu-Leu) containing 2
1427131_s_at	3.35	Lrrc58	leucine rich repeat containing 58
1454136_a_at	3.32	4921524J17Rik	RIKEN cDNA 4921524J17 gene
1434328_at	3.27	Rpl15	ribosomal protein L15
1426205_at	3.24	Ppp1cb	protein phosphatase 1, catalytic subunit, beta isoform
1436221_at	3.21	Ildr2	immunoglobulin-like domain containing receptor 2
1428853_at	3.21	Ptch1	patched homolog 1
1418392_a_at	3.20	Gbp3	guanylate binding protein 3
1454694_a_at	3.20	Top2a	topoisomerase (DNA) II alpha
1434070_at	3.19	Jag1	jagged 1
1458679_a_at	3.19	Tatdn1	TatD DNase domain containing 1
1428162_at	3.19	4933421E11Rik	RIKEN cDNA 4933421E11 gene
1456236_s_at	3.18	Comm10	COMM domain containing 10
1426222_s_at	3.18	Vwa5a	von Willebrand factor A domain containing 5A
1416988_at	3.17	Msh2	mutS homolog 2
1429454_at	3.14	Gapvd1	GTPase activating protein and VPS9 domains 1
1454689_at	3.13	Srrm1	serine/arginine repetitive matrix 1
1418372_at	3.10	Adsl	adenylosuccinate lyase
1448794_s_at	3.06	Dnajc2	DnaJ (Hsp40) homolog, subfamily C, member 2
1417974_at	3.06	Kpna4	karyopherin (importin) alpha 4
1433585_at	3.04	Tnpo1	Transportin 1
1443208_at	3.04	LOC100044979	G protein-coupled receptor 137B
1429201_at	3.01	Cyld	cylindromatosis (turban tumor syndrome)
1437276_at	3.00	N/A	N/A
1431930_x_at	2.97	Crls1	cardiolipin synthase 1
1449056_at	2.97	E330009J07Rik	RIKEN cDNA E330009J07 gene
1434513_at	2.94	Atp13a3	ATPase type 13A3
1429508_at	2.93	2310057M21Rik	RIKEN cDNA 2310057M21 gene
1421968_a_at	2.90	Nipa2	non imprinted in Prader-Willi/Angelman syndrome 2 homolog
1419076_a_at	2.90	Brca2	breast cancer 2
1435789_x_at	2.90	N/A	N/A
1434336_s_at	2.90	Rcor1	REST corepressor 1
1428681_at	2.89	Gm608	gene model 608, (NCBI)
1449039_a_at	2.88	Hnrpd1	heterogeneous nuclear ribonucleoprotein D-like
1428407_at	2.87	Hnrnpa0	heterogeneous nuclear ribonucleoprotein A0
1422553_at	2.83	Pten	phosphatase and tensin homolog
1452635_x_at	2.82	Taf1d	TATA box binding protein (Tbp)-associated factor, RNA polymerase I, D
1444139_at	2.80	Ddit4l	DNA-damage-inducible transcript 4-like
1419759_at	2.79	Abcb1a	ATP-binding cassette, sub-family B (MDR/TAP), member 1A
1424358_at	2.79	Ube2e2	ubiquitin-conjugating enzyme E2E 2
1442785_at	2.79	A130004G11Rik	RIKEN cDNA A130004G11 gene
1455024_at	2.79	Tlk1	tousled-like kinase 1
1449670_x_at	2.79	LOC100044979	G protein-coupled receptor 137B
1416614_at	2.77	Eid1	EP300 interacting inhibitor of differentiation 1
1457024_x_at	2.77	Slc35a2	solute carrier family 35 (UDP-galactose transporter), member

A2			
1419495_at	2.76	Immp2l	IMP2 inner mitochondrial membrane peptidase-like
1454846_at	2.76	Utp15	UTP15, U3 small nucleolar ribonucleoprotein, homolog
1455483_at	2.75	Zfp148	zinc finger protein 148
1454831_at	2.75	Foxn2	forkhead box N2
1418988_at	2.75	Pex7	peroxisomal biogenesis factor 7
1451649_a_at	2.74	Wdr75	WD repeat domain 75
1455513_at	2.74	Taf1	TAF1 RNA polymerase II, TATA box binding protein (TBP)-associated factor
1424156_at	2.73	Rbl1	retinoblastoma-like 1 (p107)
1415863_at	2.73	Eif4g2	eukaryotic translation initiation factor 4, gamma 2
1429438_at	2.72	Bcor	BCL6 interacting corepressor
1440187_at	2.71	Taf3	TAF3 RNA polymerase II, TATA box binding protein (TBP)-associated factor
1424495_a_at	2.70	Cklf	chemokine-like factor
1429043_at	2.70	Smndc1	survival motor neuron domain containing 1
1429796_at	2.70	Kalrn	kalirin, RhoGEF kinase
1442757_at	2.70	Lrch1	leucine-rich repeats and calponin homology (CH) domain containing 1
1416860_s_at	2.70	Ing1	inhibitor of growth family, member 1
1415890_at	2.69	Papss1	3'-phosphoadenosine 5'-phosphosulfate synthase 1
1451641_at	2.68	Dbr1	debranching enzyme homolog 1
1415791_at	2.67	Rnf34	ring finger protein 34
1449175_at	2.66	Gpr65	G-protein coupled receptor 65
1428087_at	2.64	Dnm1l	dynamitin 1-like
1435821_s_at	2.63	Ppp1r8	protein phosphatase 1, regulatory (inhibitor) subunit 8
1417770_s_at	2.63	Psmc6	proteasome (prosome, macropain) 26S subunit, ATPase, 6
1422857_at	2.63	Trip4	thyroid hormone receptor interactor 4
1439994_at	2.63	1810013D10Rik	RIKEN cDNA 1810013D10 gene
1454998_at	2.63	1200011I18Rik	
1451374_x_at	2.63	Cklf	chemokine-like factor
1415737_at	2.62	Rfk	riboflavin kinase
1451745_a_at	2.62	Znht1	zinc finger, HIT domain containing 1
1434418_at	2.62	Cers6	ceramide synthase 6
1426977_at	2.60	Usp47	ubiquitin specific peptidase 47
1438055_at	2.60	Rarres1	retinoic acid receptor responder (tazarotene induced) 1
1454938_at	2.59	Snx13	sorting nexin 13
1456886_at	2.59	N/A	N/A
1451000_at	2.59	Tmem126a	transmembrane protein 126A
1416653_at	2.58	Stxbp3a	syntrophin binding protein 3A
1448234_at	2.55	Dnajb6	DnaJ (Hsp40) homolog, subfamily B, member 6
1435901_at	2.55	Usp40	ubiquitin specific peptidase 40
1424782_at	2.55	Tmem77	transmembrane protein 77
1428552_at	2.54	2610001J05Rik	RIKEN cDNA 2610001J05 gene
1450012_x_at	2.53	Ywhag	tyrosine 3-monooxygenase/tryptophan 5-monooxygenase activation protein, gamma polypeptide
1418180_at	2.53	Sp1	trans-acting transcription factor 1

1416952_at	2.53	Atp6v1d	ATPase, H ⁺ transporting, lysosomal V1 subunit D
1448589_at	2.53	Ndufb5	NADH dehydrogenase (ubiquinone) 1 beta subcomplex, 5
1459657_s_at	2.53	Polr1d	predicted gene, OTTMUSG00000008305
1417564_at	2.53	Med7	mediator complex subunit 7
1444328_at	2.52	Clta	clathrin light chain 3
1429559_at	2.52	Gnaq	guanine nucleotide binding protein, alpha q polypeptide
1423707_at	2.52	Tmem50b	transmembrane protein 50B
1417507_at	2.51	Cyb561	cytochrome b-561
1455915_at	2.51	Galnt4	UDP-N-acetyl-alpha-D-galactosamine:polypeptide N-acetylglucosaminyltransferase 4
1452130_at	2.50	Txndc14	thioredoxin domain containing 14
1425074_at	2.49	Wrn	Werner syndrome homolog
1417594_at	2.49	Gkap1	G kinase anchoring protein 1
1452152_at	2.48	Clint1	clathrin interactor 1
1435093_at	2.48	Zfyve20	zinc finger, FYVE domain containing 20
1440310_at	2.47	Runx1t1	runt-related transcription factor 1; translocated to, 1 (cyclin D-related)
1441315_s_at	2.47	Slc19a2	solute carrier family 19 (thiamine transporter), member 2
1436796_at	2.47	Matr3	matrin 3
1451195_a_at	2.46	Tmx1	thioredoxin-related transmembrane protein 1
1436272_at	2.45	Rab3gap2	RAB3 GTPase activating protein subunit 2
1436945_x_at	2.45	Stim1	stromal interaction molecule 1
1435754_at	2.45	Zyg11b	zyg-11 homolog B
1419208_at	2.45	Map3k8	mitogen-activated protein kinase kinase kinase 8
1426842_at	2.45	Ythdf3	YTH domain family 3
1417365_a_at	2.43	Calm1	calmodulin 1
1435284_at	2.43	Rtn4	reticulon-4
1447776_x_at	2.43	Rab6	RAB6, member RAS oncogene family
1434389_at	2.43	Sos1	son of sevenless homolog 1
1415963_at	2.42	Hnrnp2	heterogeneous nuclear ribonucleoprotein H2
1438306_at	2.42	Rnf180	ring finger protein 180
1419453_at	2.41	Uchl5	ubiquitin carboxyl-terminal esterase L5
1422748_at	2.41	Zeb2	zinc finger E-box binding homeobox 2
1429436_at	2.40	Prpf40a	pre-mRNA processing factor 40 homolog A
1455252_at	2.39	Tsc1	tuberous sclerosis 1
1423994_at	2.38	Kif1b	kinesin family member 1B
1455505_at	2.37	Gatad2a	GATA zinc finger domain containing 2A
1416009_at	2.35	Tspan3	tetraspanin 3
1454602_s_at	2.34	Cnot2	CCR4-NOT transcription complex, subunit 2
1455658_at	2.33	Cggbp1	CGG triplet repeat binding protein 1
1448733_at	2.32	Bmi1	Bmi1 polycomb ring finger oncogene
1424147_at	2.32	Ahsa1	AHA1, activator of heat shock protein ATPase homolog 1
1433898_at	2.32	N/A	N/A
1433668_at	2.32	Pnrc1	proline-rich nuclear receptor coactivator 1
1424111_at	2.32	Igf2r	insulin-like growth factor 2 receptor
1434437_x_at	2.32	Rrm2	ribonucleotide reductase M2

1424043_at	2.31	Ppil4	peptidylprolyl isomerase (cyclophilin)-like 4
1439345_at	2.31	Gpnmb	glycoprotein (transmembrane) nmb
1439463_x_at	2.31	LOC637733	predicted gene, EG665056
1440339_at	2.31	Enpp1	ectonucleotide pyrophosphatase/phosphodiesterase 1
1428252_at	2.31	Chmp2b	chromatin modifying protein 2B
1451971_at	2.30	Cul4a	cullin 4A
1422449_s_at	2.30	Rcn2	reticulocalbin 2
1417478_a_at	2.30	Ppp2r3c	protein phosphatase 2, regulatory subunit B'', gamma
1434937_at	2.30	Mycbp2	MYC binding protein 2
1415682_at	2.29	Xpo7	exportin 7
1433755_at	2.29	Mier1	mesoderm induction early response 1 homolog
1434317_s_at	2.28	Tex10	testis expressed gene 10
1423266_at	2.28	2810405K02Rik	RIKEN cDNA 2810405K02 gene
1430404_at	2.27	4833416J08Rik	A kinase (PRKA) anchor protein 13
1426877_a_at	2.26	Pbrm1	polybromo 1
1451356_at	2.26	Anp32e	acidic (leucine-rich) nuclear phosphoprotein 32 family, member E
1437386_at	2.26	Lingo1	leucine rich repeat and Ig domain containing 1
1434352_at	2.25	B630005N14Rik	RIKEN cDNA B630005N14 gene
1416267_at	2.24	Scoc	short coiled-coil protein
1423069_at	2.24	Adnp	activity-dependent neuroprotective protein
1418443_at	2.23	Xpo1	exportin 1, CRM1 homolog
1455031_at	2.22	Cdc2l6	cell division cycle 2-like 6 (CDK8-like)
1459219_at	2.21	Rapgef2	Rap guanine nucleotide exchange factor (GEF) 2
1456019_at	2.18	Cwf19l2	CWF19-like 2, cell cycle control
1448304_a_at	2.18	Rab6	RAB6, member RAS oncogene family
1437892_at	2.17	Zkscan3	zinc finger with KRAB and SCAN domains 3
1434928_at	2.17	Gas2l1	growth arrest-specific 2 like 1
1416637_at	2.16	Slc4a2	solute carrier family 4 (anion exchanger), member 2
1436732_s_at	2.16	Fbxw8	F-box and WD-40 domain protein 8
1458662_at	2.15	Daam1	RIKEN cDNA 1700008O03 gene
1453109_at	2.15	Arsk	arylsulfatase K
1421910_at	2.15	Tcf20	transcription factor 20
1416247_at	2.14	Dctn3	dynactin 3
1454863_at	2.12	Ankrd11	ankyrin repeat domain 11
1417995_at	2.12	Ptpn22	protein tyrosine phosphatase, non-receptor type 22
1418736_at	2.11	B3galnt1	UDP-GalNAc:betaGlcNAc beta 1,3-galactosaminyltransferase, polypeptide 1
1433740_at	2.10	Tmem87b	transmembrane protein 87B
1455312_at	2.09	Phc3	polyhomeotic-like 3
1416477_at	2.08	Ube2d2	ubiquitin-conjugating enzyme E2D 2
1427134_at	2.08	Sfrs12	splicing factor, arginine/serine-rich 12
1438769_a_at	2.07	Thyn1	thymocyte nuclear protein 1
1425018_at	2.07	Mcts1	malignant T cell amplified sequence 1
1457069_at	2.06	Ascc3	activating signal cointegrator 1 complex subunit 3
1428949_at	2.05	Xpot	exportin, tRNA (nuclear export receptor for tRNAs)

1429588_at	2.04	2810474O19Rik	RIKEN cDNA 2810474O19 gene
1448509_at	2.04	Fam107b	family with sequence similarity 107, member B
1422675_at	2.03	Smarce1	SWI/SNF related, matrix associated, actin dependent regulator of chromatin, subfamily e, member 1
1448398_s_at	2.03	Rpl22	ribosomal protein L22
1435988_x_at	2.02	Ik	IK cytokine
1417390_at	2.02	Gpn1	GPN-loop GTPase 1
1448215_a_at	2.01	Dpp3	dipeptidylpeptidase 3
1421965_s_at	2.01	Notch3	Notch gene homolog 3
1424842_a_at	2.01	Arhgap24	Rho GTPase activating protein 24
1434014_at	2.01	Atg4c	autophagy-related 4C
1435347_at	1.99	Stau1	staufen (RNA binding protein) homolog 1
1421077_at	1.99	Sertad3	SERTA domain containing 3
1428461_at	1.99	Ppp2r5e	protein phosphatase 2, regulatory subunit B (B56), epsilon isoform
1436165_at	1.98	Luc7l2	LUC7-like 2
1452895_at	1.98	Fbxo45	F-box protein 45
1455728_at	1.98	Pten	phosphatase and tensin homolog
1456617_a_at	1.97	Eif2s2	eukaryotic translation initiation factor 2, subunit 2
1436977_at	1.97	N/A	N/A
1448527_at	1.97	Pdcd10	programmed cell death 10
1458414_at	1.96	D2Ertd93e	DNA segment, Chr 2, ERATO Doi 93, expressed
1420528_at	1.95	Gpatch2	G patch domain containing 2
1460615_at	1.95	Nt5dc1	5'-nucleotidase domain containing 1
1449085_at	1.95	Phf10	PHD finger protein 10
1431694_a_at	1.95	Ctnnbip1	catenin beta interacting protein 1
1416840_at	1.93	Mid1ip1	Mid1 interacting protein 1
1449694_s_at	1.93	Comm5	COMM domain containing 5
1455432_at	1.92	Taok1	TAO kinase 1
1434561_at	1.92	Asxl1	additional sex combs like 1
1426844_a_at	1.92	Pdcd2l	programmed cell death 2-like
1416998_at	1.91	Rrs1	RRS1 ribosome biogenesis regulator homolog
1427156_s_at	1.88	Ascc2	activating signal cointegrator 1 complex subunit 2
1424389_at	1.86	Nupl1	nucleoporin like 1
1435389_at	1.86	Reps2	RALBP1 associated Eps domain containing protein 2
1423167_at	1.86	Mobk3	MOB1, Mps One Binder kinase activator-like 3
1453104_at	1.86	Mapk1	mitogen-activated protein kinase 1
1455403_at	1.84	Manea	mannosidase, endo-alpha
1436346_at	1.82	Cd109	CD109 antigen
1438771_at	1.81	LOC100045983	bromodomain containing 1
1455644_at	1.80	Vps53	vacuolar protein sorting 53
1424991_s_at	1.80	Tyms-ps	thymidylate synthase
1441942_x_at	1.80	Snupn	snurportin 1
1427317_at	1.79	Kin	antigenic determinant of rec-A protein
1428254_at	1.79	Purb	purine rich element binding protein B
1426840_at	1.78	Ythdf3	YTH domain family 3

1453030_at	1.77	Msl2	male-specific lethal 2 homolog
1425542_a_at	1.77	Ppp2r5c	protein phosphatase 2, regulatory subunit B (B56), gamma isoform
1416668_at	1.77	Ttc35	tetratricopeptide repeat domain 35
1423385_at	1.75	Actr8	ARP8 actin-related protein 8 homolog
1428144_at	1.74	Lrwd1	leucine-rich repeats and WD repeat domain containing 1
1448391_at	1.73	Rab9	RAB9, member RAS oncogene family
1416280_at	1.70	Uba2	ubiquitin-like modifier activating enzyme 2
1418483_a_at	1.66	Ggta1	glycoprotein galactosyltransferase alpha 1, 3
1430221_at	1.64	9130008F23Rik	
1426625_at	1.63	Zfp623	zinc finger protein 623
1430805_s_at	1.63	Rmi1	RMI1, RecQ mediated genome instability 1, homolog
1452110_at	1.62	Mtrr	5-methyltetrahydrofolate-homocysteine methyltransferase reductase
1455465_at	1.62	N/A	N/A
1415765_at	1.61	Hnrnpul2	heterogeneous nuclear ribonucleoprotein U-like 2
1452262_at	1.60	Grpel2	GrpE-like 2, mitochondrial
1417305_at	1.59	Speg	SPEG complex locus
1433749_at	1.56	Gna13	guanine nucleotide binding protein, alpha 13
1435169_at	1.55	A930001N09Rik	
1423964_at	1.55	Cpsf3l	cleavage and polyadenylation specific factor 3-like
1457724_at	1.54	Ctsl	cathepsin L
1416641_at	1.53	Lig1	ligase I, DNA, ATP-dependent
1449614_s_at	1.52	AI314976	expressed sequence AI314976
1442004_at	1.51	Trim65	tripartite motif-containing 65
1434697_at	1.51	Ddx6	DEAD (Asp-Glu-Ala-Asp) box polypeptide 6
1423465_at	1.50	LOC100046401	ferric-chelate reductase 1
1416768_at	1.45	1110003E01Rik	RIKEN cDNA 1110003E01 gene
1454195_at	1.38	4933433G19Rik	
1453412_a_at	1.36	Sec14l1	SEC14-like 1 (S. cerevisiae)
1454837_at	1.36	Cln6	ceroid-lipofuscinosis, neuronal 6
1451310_a_at	1.12	Ctsl	cathepsin L
1448513_a_at	1.05	Npc2	Niemann Pick type C2
1436928_s_at	-1.32	Adcy3	adenylate cyclase 3
1435452_at	-1.37	Tmem20	transmembrane protein 20
1426166_at	-1.37	Mup5	major urinary protein 5
1443177_at	-1.38	N/A	N/A
1419970_at	-1.38	Slc35a5	solute carrier family 35, member A5
1436425_at	-1.39	Kank4	KN motif and ankyrin repeat domains 4
1421472_at	-1.40	2900083I11Rik	RIKEN cDNA 2900083I11 gene
1427713_x_at	-1.40	Pou2f2	POU domain, class 2, transcription factor 2
1439025_at	-1.45	Zfp446	zinc finger protein 446
1459247_at	-1.45	Agbl3	ATP/GTP binding protein-like 3
1445662_x_at	-1.47	N/A	N/A
1459182_at	-1.51	N/A	N/A
1450176_at	-1.51	Ern1	endoplasmic reticulum (ER) to nucleus signalling 1

1446354_at	-1.53	C130098B18Rik	RIKEN cDNA C130098B18 gene
1429560_at	-1.53	100043468	predicted gene, 100043468
1440722_at	-1.55	D19Ert386e	
1459324_at	-1.58	Fermt2	fermitin family homolog 2
1419214_at	-1.59	Tnfrsf11a	tumor necrosis factor receptor superfamily, member 11a
1438529_at	-1.60	Tmem201	transmembrane protein 201
1445175_at	-1.61	100042940	predicted gene, 100042940
1443785_x_at	-1.62	Pdlim7	PDZ and LIM domain 7
1433099_at	-1.63	4933428L12Rik	RIKEN cDNA 4933428L12 gene
1452764_at	-1.65	Socs6	suppressor of cytokine signaling 6
1454294_at	-1.66	2310061A09Rik	RIKEN cDNA 2310061A09 gene
1432156_a_at	-1.66	Rnf32	ring finger protein 32
1458747_at	-1.66	Fbxo45	F-box protein 45
1432260_at	-1.67	Gpr39	G protein-coupled receptor 39
1448000_at	-1.70	Cdca3	cell division cycle associated 3
1459307_at	-1.71	N/A	N/A
1432875_at	-1.72	4632409D06Rik	RIKEN cDNA 4632409D06 gene
1455961_at	-1.72	Mme	membrane metallo endopeptidase
1447884_x_at	-1.73	Fam134c	family with sequence similarity 134, member C
1458661_at	-1.73	N/A	N/A
1430137_at	-1.74	1300002E11Rik	RIKEN cDNA 1300002E11 gene
1439515_at	-1.75	Setd5	SET domain containing 5
1456045_at	-1.76	1700106N22Rik	RIKEN cDNA 1700106N22 gene
1439339_at	-1.76	N/A	N/A
1447789_x_at	-1.77	Ddx6	DEAD (Asp-Glu-Ala-Asp) box polypeptide 6
1436267_a_at	-1.78	Frap1	FK506 binding protein 12-rapamycin associated protein 1
1441626_at	-1.78	N/A	N/A
1435627_x_at	-1.79	N/A	N/A
1423224_at	-1.82	Tctn2	tectonic family member 2
1443719_x_at	-1.82	Ddx42	DEAD (Asp-Glu-Ala-Asp) box polypeptide 42
1437594_x_at	-1.83	Pigt	phosphatidylinositol glycan anchor biosynthesis, class T
1457639_at	-1.83	Atp6v1h	V-ATPase subunit H
1430996_at	-1.85	Etnk1	ethanolamine kinase 1
1420769_at	-1.86	Dhx58	DEXH (Asp-Glu-X-His) box polypeptide 58
1425901_at	-1.87	Nfatc2	nuclear factor of activated T-cells, cytoplasmic, calcineurin-dependent 2
1447377_at	-1.87	Gm428	
1453090_x_at	-1.88	N/A	N/A
1421990_at	-1.90	Syt1	synaptotagmin I
1452920_a_at	-1.96	Ppil2	peptidylprolyl isomerase (cyclophilin)-like 2
1423953_at	-1.96	Cdkal1	CDK5 regulatory subunit associated protein 1-like 1
1432711_at	-1.96	4933425M03Rik	
1457629_at	-1.97	Atmin	ATM interactor
1415748_a_at	-1.97	Dctn5	polo-like kinase 1
1430358_at	-1.99	Becn1	beclin 1
1430373_at	-1.99	5430427O19Rik	RIKEN cDNA 5430427O19 gene

1447820_x_at	-2.00	Cpt2	carnitine palmitoyltransferase 2
1437762_at	-2.04	Rab39	RAB39, member RAS oncogene family
1416787_at	-2.07	Acvr1	activin A receptor, type 1
1446422_at	-2.12	A530081L18Rik	membrane-associated ring finger (C3HC4) 3
1447267_at	-2.14	C85319	expressed sequence C85319
1454219_at	-2.15	Dnajc2	DnaJ (Hsp40) homolog, subfamily C, member 2
1430772_at	-2.22	4932438H23Rik	RIKEN cDNA 4932438H23 gene
1447768_at	-2.24	Got2	glutamate oxaloacetate transaminase 2, mitochondrial
1446001_at	-2.25	N/A	N/A
1442954_at	-2.33	N/A	N/A
1444873_at	-2.35	Hip1	huntingtin interacting protein 1
1424595_at	-2.37	F11r	F11 receptor
1455284_x_at	-2.41	Pigx	phosphatidylinositol glycan anchor biosynthesis, class X
1420948_s_at	-2.42	Atrx	alpha thalassemia/mental retardation syndrome X-linked homolog
1441784_at	-2.46	N/A	N/A
1446211_at	-2.55	ErbB4	v-erb-a erythroblastic leukemia viral oncogene homolog 4
1433020_at	-2.65	5830413G11Rik	RIKEN cDNA 5830413G11 gene
1456808_at	-2.68	4933426M11Rik	RIKEN cDNA 4933426M11 gene
1453534_at	-2.71	2810004I08Rik	
1446004_at	-2.95	N/A	N/A
1452240_at	-3.25	Bruno14	bruno-like 4, RNA binding protein